Contribution from the Research School of Chemistry,
Australian National University, GPO Box 4, Canberra, ACT 2601, Australia

Stepwise Ligand-Additivity Effects on Electrode Potentials and Charge-Transfer Spectra in Hexahalide, Mixed Halide/Nitrile, and Hexakis(nitrile) Complexes of Ruthenium(IV), -(III), and -(II)

Colleen M. Duff† and Graham A. Heath*

Received December 27, 1989

This paper examines complete series of substituted ruthenium halide complexes ranging stepwise from $[RuX_6]^{2-}$ through $[RuX_{6-n}(RCN)_n]^z$ to $[Ru(RCN)_6]^{2+}$ in order to define the variation in electrode potentials ($Ru^{V/IV}$, $Ru^{IV/III}$, and $Ru^{III/II}$) and the accompanying trends in both halide-to-metal and metal-to-nitrile charge-transfer spectra. Three series are described: X = Cl^-, RCN = PhCN; X = Cl^-, RCN = MeCN; and X = Br^-, RCN = PhCN. Voltammetric studies show that the metal-based electrode potentials are a linear function of stoichiometry: the effect on $E_{1/2}$ of replacing each halide by nitrile is consistently +0.6 V for $Ru^{III/II}$ and $Ru^{IV/III}$ and +0.45 V for $Ru^{V/IV}$. For $[MX_{6-n}(RCN)_n]^z$ complexes in general, the same dependence of electrode potentials on stoichiometry is shared by congeneric $4d^n$ and $5d^n$ metal ions such as Ru and Os and by isovalent metal ions as diverse as Ru^{IV} and Nb^{IV}. These measurements consolidate and extend the application of additive ligand electrochemical parameters. For the $[MCl_6]^{2-}$ complexes of 4d and 5d transition metals, with M^{IV} ranging from Mo to Rh and from W to Ir, the halide-to-metal charge-transfer energies are shown to be linearly dependent on the appropriate electrode potentials, $E_{1/2}(M^{IV/III})$. For each complex in the $[RuX_{6-n}(RCN)_n]^z$ series, the charge-transfer spectra have been recorded in all accessible oxidation states (Ru^{IV}, Ru^{III}, and Ru^{II}) by spectroelectrochemical measurements. The progressions in LMCT and MLCT band positions with stepwise substitution are complementary to the trend in the appropriate metal-based electrode potentials. Compilation of the electrochemical and spectroscopic data yields a conceptual representation of the relative frontier-orbital energies of ruthenium, halide, and nitrile as a function of stoichiometry.

Introduction

Comprehensive investigation of 4d and 5d transition-metal hexafluorides and hexachlorides (Zr to Pd and Hf to Pt) has revealed a rich pattern of reversible redox couples $[MX_6]^{z/z-1}$ ($z = 0, -1, -2$) with the successive $E_{1/2}$ values following orderly trends across each series related to central ion core-charge and inter-electronic correlation terms.[1,2] Recognition of these important periodic progressions for the hexahalometalates prompted us to seek similarly rational patterns in the electronic properties of the general category of complexes with the stoichiometry $MX_{6-n}L_n$. That is, we expect similar patterns in $E_{1/2}$ for substituted complexes of a specific stoichiometry containing an invariant neutral ligand L, as M varies across the periodic table. For such patterns to occur it is necessary that common to all these metals should be a systematic descent in electrode potential from MX_6, through $MX_{6-n}L_n$ to ML_6. This corollary is the focus of the present paper.

Here we report on the electrochemistry and optical spectra of exhaustive series of nitrile-substituted ruthenium complexes $[RuX_{6-n}(RCN)_n]^z$ (R = Ph or Me; X = Br^- or Cl^-), with n ranging stepwise from 0 to 6. Each complex was derived from $[RuX_6]^{2-}$ by successive electrochemically induced halide displacements ($n = 1-4$), followed by chemically promoted halide abstraction ($n = 5, 6$).[3] The voltammetric survey of these seven-membered series reveals a notably strict linear and parallel dependence of the $Ru^{IV/III}$ and $Ru^{III/II}$ redox couples on the number of halide ligands. For each stoichiometry, we describe the electronic charge-transfer spectra in all accessible oxidation states Ru^{IV}, Ru^{III}, or Ru^{II}. Throughout each $[MX_{6-n}(RCN)_n]^z$ series the behavior of the charge-transfer spectra is complementary to the progression in electrode potentials. That is, the absorption energies for both LMCT ($X \rightarrow Ru^{III}$ or $X \rightarrow Ru^{IV}$) and MLCT ($Ru^{II} \rightarrow RCN$) bands are shown to vary in an orderly way with the degree of halide ligation. A preliminary account of this work has been given elsewhere.[4]

The existence of systematic ligand additivity effects in relation to metal-based electrode potentials is receiving increasing recognition. Chatt and Pickett assigned quantitative ligand parameters (P_L) based on shifts in the d^5/d^6 couples of $Cr(CO)_5L$ and $M(dppe)_2LL'$ complexes (M = Mo, Re, Fe).[5] Bursten has provided a formal ligand-field analysis, together with a general review of ligand additivity in metal carbonyl derivatives and several related systems.[6] Datta has demonstrated that ligand additivity effects, as defined by P_L, likewise prevail in $Ru(bpy)_2LL'$ complexes[7] and has discussed the relationship between the Chatt and Bursten parameterizations.

Of particular relevance to this work are the less extensive series $[MCl_{6-n}(MeCN)_n]^z$ (M = Nb, Ta; $n = 0-2$)[8] and $[OsCl_{6-n}(py)_n]^z$ ($n = 0-4$)[9] and also the dinuclear systems $[Ru_2(\mu\text{-}Cl_3)Cl_{6-n}L_n]^z$,[10] which exhibit equally systematic linear trends in metal-based electrode potentials upon replacement of halide ions by neutral ligands. Since the submission of the present paper, an extensive collation of voltammetric data by Lever has appeared in which a new electrochemical parameter scale for numerous ligands is derived from ligand-additivity relationships.[11]

The possible utility of combining electrochemical and charge-transfer spectroscopic data is receiving renewed attention.[12] It has been demonstrated repeatedly that the metal to ligand charge-transfer transition energy varies linearly with the measured difference in metal and ligand electrode potentials for ruthenium and osmium bipyridyls and related complexes.[13,14] This paper

† Current address: Department of Chemistry, University of New South Wales, Australian Defence Force Academy, Canberra, ACT 2600, Australia.

(1) Brownstein, S.; Heath, G. A.; Sengupta, A.; Sharp, D. W. A. *J. Chem. Soc., Chem. Commun.* **1983**, 669.
(2) Heath, G. A.; Moock, K. A.; Sharp, D. W. A.; Yellowlees, L. J. *J. Chem. Soc., Chem. Commun.* **1985**, 15.
(3) Duff, C. M.; Heath, G. A. *J. Chem. Soc., Dalton Trans.*, in press.
(4) Duff, C. M.; Heath, G. A. Presented at the XXVIIth International Conference on Coordination Chemistry, Broadbeach, Australia, 1989; Abstract W40.
(5) Chatt, J.; Kan, C. T.; Leigh, G. J.; Pickett, C. J.; Stanley, D. R. *J. Chem. Soc., Dalton Trans.* **1980**, 2032.
(6) (a) Bursten, B. E. *J. Am. Chem. Soc.* **1982**, *104*, 1299. (b) Bursten, B. E.; Darensbourg, D. J.; Kellogg, G. E.; Lichtenberger, D. L. *Inorg. Chem.* **1984**, *23*, 4361. (c) Bursten, B. E.; Green, M. R. *Prog. Inorg. Chem.* **1988**, *36*, 425.
(7) Datta, D. *J. Chem. Soc., Dalton Trans.* **1986**, 1907.
(8) Bursten, B. E.; Green, M. R.; Katović, V.; Kirk, J. R.; Lightner, D., Jr. *Inorg. Chem.* **1986**, *25*, 831.
(9) Yellowlees, L. J.; Taylor, K. J. Presented at the XXVIIth International Conference on Coordination Chemistry, Broadbeach, Australia, 1989; Abstract W35.
(10) Coombe, V. T.; Heath, G. A.; Stephenson, T. A.; Vattis, D. K. *J. Chem. Soc., Dalton Trans.* **1983**, 2307.
(11) Lever, A. B. P. *Inorg. Chem.* **1990**, *29*, 1271. This paper appeared after the original submission of our manuscript, and the discussion of E_L is added in response.
(12) (a) Lever, A. B. P. *Inorganic Electronic Spectroscopy*, 2nd ed.; Elsevier: New York, 1986; p 776. (b) Saji, T.; Aoyagui, S. *J. Electroanal. Chem. Interfacial Electrochem.* **1975**, *60*, 1. (c) Shriver, D. F.; Posner, J. *J. Am. Chem. Soc.* **1966**, *88*, 1672. (d) Barnes, J. C.; Day, P. *J. Chem. Soc.* **1964**, 3886. (e) Dainton, F. S. *J. Chem. Soc.* **1952**, 1533.

0020-1669/91/1330-2528$02.50/0

reports that a corresponding and equally systematic relationship exists between ligand to metal charge-transfer energies and central ion reduction potentials in $[MCl_6]^{2-}$ complexes containing a wide range of 4d and 5d metals.[15] In addition, with the progressively substituted mixed halide/nitrile compounds at our disposal, we are able to show simultaneously that empirical $h\nu - \Delta E_{1/2}$ relationships prevail for *both* LMCT and MLCT spectra in the mixed halide/nitrile complexes. It is then possible to compile the optical and electrochemical data so as to map the relative metal and ligand frontier-orbital energies in each $[RuX_{6-n}(RCN)_n]^z$ complex. Defined in this way, the frontier orbital domain (Ru $d\pi$, Cl^- or Br^- π, and RCN π^*) is shown to change dramatically as n increases from 0 to 6.

Experimental Section

Voltammetry. Variable-temperature voltammetric measurements were conducted in CH_2Cl_2 or in mixed RCN (≤20%)/CH_2Cl_2 solvent systems, 0.5 M in Bu_4NBF_4, by using a PAR 170 electrochemistry system and a standard three-electrode configuration. The required solvents were distilled from appropriate drying agents under N_2 immediately before use. The electrolyte was recrystallized from ethyl acetate/ether and dried in stages (room temperature to 100 °C) under vacuum until a satisfactory voltammetric range was achieved (±2 V in CH_2Cl_2). The nonaqueous reference electrode was of the form [Ag|AgCl|(CH_2Cl_2/0.05 M Bu_4NCl, 0.45 M Bu_4NBF_4)] and was constructed from a Metrohm 24-140 Ag/AgCl assembly separated by a fritted salt bridge. The reference electrode was maintained at room temperature during voltammetric measurements, the thermal gradient being within the salt bridge. Under these conditions the oxidation of ferrocene is observed at +0.56 V at 20 °C and was found to vary by no more than 30 mV between −70 and 20 °C and over the range of mixed CH_2Cl_2/RCN solvents. Linear dc voltammograms employed a Tacussel EDI rotating platinum electrode (rpe) in the range 1000–6000 rpm, while cyclic and ac voltammograms employed 1-mm Pt-disk working electrodes. Routine scan rates were 100 and 200 mV s^{-1} in cyclic voltammetry and 10 mV s^{-1} in other modes, with positive-feedback resistance compensation and phase-sensitive detection (ω = 200 Hz) in ac measurements. Solutions were typically 10^{-3} M in complex and were purged with Ar to exclude Ru^{II}/N_2 coordination. Cell temperatures were maintained by immersion in a constant-temperature bath and were monitored by a digital thermometer probe within the cell solution. The measured potentials were corrected for the influence of temperature and solvent variation by cross reference to internal redox standards, $(Bu_4N)_2[RuX_6]$, $(Bu_4N)[RuX_4(RCN)_2]$, or $[Fe(C_5H_5)_2]$, as described below.

Charge-Transfer Spectra. The electronic absorption spectra in the range 45 000–10 000 cm^{-1} were recorded with a Perkin-Elmer Lambda 9 double-beam spectrometer operating in linear wavenumber mode with digital background subtraction. Accessible oxidized and reduced species were characterized by electrogeneration in a chilled optically transparent electrochemical cell mounted in the spectrometer. This cell is of one-piece fused-silica construction and embodies a conventional-geometry 0.5-mm path length optical cuvette (Suprasil W) expanding to a tubular upper section to accommodate the counter and reference electrode assemblies. The electrolyte solution is prepurged of O_2 and introduced by syringe. The platinum spiral counterelectrode and the Ag/AgCl reference electrode are both isolated by frits, and the reference electrode is maintained at ambient temperature. The working electrode is a 40 mm × 9 mm rectangular section Pt gauze of 70% transmittance located centrally in the optical beam.

The generation potential is set 150 mV beyond $E_{1/2}$ to achieve ca. 99% conversion. Typically, electrolysis is complete within minutes in the thin-layer region of the cell, in contrast to the "instantaneous" Nernstian equilibration expected of an idealized thin-layer electrode (OTTLE) cell of sandwich construction and path length <0.1 mm. This consideration is far outweighed by the operational advantages of having a stable leak-free cell in the present application, working with sensitive compounds in nonaqueous solvents over a wide temperature range. The macroscopic path length also yields superior optical densities at convenient concentrations. The cell is mounted in a cryostatic cell block fitted with gas ports and is chilled by a flow of cold dry N_2 as commonly employed in ESR/NMR technology. Temperatures in the range 0 to −80 °C are maintained precisely by an automatic Bruker B-VT 1000 control unit. Thermal fluctuations greater than ±2 °C are sufficient to disrupt isosbestic optical density measurements because of the associated variation in solution volume.

Table I. Electrochemical Data for $[RuX_{6-n}(RCN)_n]^{z/z-}$, Measured vs Ag/AgCl[a] under the Conditions Indicated[b-g]

n	V/IV	IV/III	III/II
	X = Cl^-, L = PhCN		
0[b]	1.78	0.22	−1.51
1[c]	2.23	0.86	−0.80[f]
2[b]		1.45	−0.27
3[d]		2.03	0.39
4[b]			1.02
5[e]			1.60
6[e]			2.23
	X = Cl^-, L = MeCN		
0[b]	1.78	0.22	−1.51
1[c]	2.20	0.82	
2[b]		1.45	−0.38
3[d]		1.89	0.29
4[d]			0.84
	X = Br^-, L = PhCN		
0[b]		0.14	−1.46[f]
1[d]		0.78	
2[b]		1.41	−0.15
3[d]			0.38
4[b]			0.97
5[e]			1.55
6[e]			2.23

[a] The $E_{1/2}$ values listed here, recorded as described in CH_2Cl_2 vs Ag/AgCl, can be compared with electrode potentials measured vs common reference electrodes in CH_3CN at ambient temperature, as follows: values in CH_3CN are estimated to be ~65 mV more positive when referred to the NHE, ~180 mV less positive when referred to the SCE, and ~600 mV less positive when referred to Fc/Fc^+ (see E_L correlation discussion and ref 11). [b] CH_2Cl_2 at −70 °C. [c] 10% RCN/CH_2Cl_2 at −30 °C. [d] 20% RCN/CH_2Cl_2 at −30 °C. [e] CH_2Cl_2 at room temperature. [f] $E_{1/2}$ was estimated from the cathodic peak. [g] Measured by cyclic and ac voltammetry, in 0.5 M Bu_4NBF_4; all values internally cross-referenced to $[RuX_6]^{2-/3-}$ and/or $[RuX_4(RCN)_2]^{1-/2-}$ (see text).

Table II. Measured Shifts in Electrode Potential for V/IV, IV/III, and II/II Couples of Nitrile-Substituted Metal Halide Complexes $[MX_{6-n}(RCN)_n]^{z/z-1}$ (Volts per Halide Displaced)[a]

complex	V/IV	IV/III	III/II
$[RuCl_{6-n}(PhCN)_n]^z$	0.45	0.60	0.62
$[RuCl_{6-n}(MeCN)_n]^z$	0.43	0.57	0.59
$[RuBr_{6-n}(PhCN)_n]^z$		0.64	0.59
$[OsBr_{6-n}(PhCN)_n]^z$ [17]	0.43	0.58	
$[NbCl_{6-n}(MeCN)_n]^z$ [8]	0.45		
$[TaCl_{6-n}(MeCN)_n]^z$ [8]	0.50		

[a] Consult Results for the precision of the ruthenium slopes.

Results

Voltammetry. Table I presents the $E_{1/2}$ data for each of the 18 complexes studied, comprising two complete series (n = 0–6, L = PhCN, and X = Cl^- or Br^-), and an incomplete series (n = 0–4, L = MeCN, and X = Cl^-). In each series, the compounds of stoichiometry $RuX_5(RCN)$ to $RuX_2(RCN)_4$ were electrogenerated in turn from $[RuX_6]^{2-}$, as described elsewhere.[3] Throughout this work $[RuCl_4(RCN)_2]^-$, $[RuCl_3(RCN)_3]$, and $[RuCl_2(RCN)_4]$ were encountered only as their respective trans, *mer*, and trans isomers, as confirmed by X-ray and spectroscopic data.[3,16] Nor was there any indication of redox-linked isomerization, even on electrosynthetic time scales.

(13) (a) Dodsworth, E. S.; Lever, A. B. P. *Chem. Phys. Lett.* **1985**, *119*, 61. (b) Ohsawa, Y.; Hanck, K. W.; DeArmond, K. *J. Electroanal. Chem. Interfacial Electrochem.* **1984**, *175*, 229. (c) Curtis, J. C.; Sullivan, B. P.; Meyer, T. J. *Inorg. Chem.* **1983**, *22*, 225.
(14) Johnson, S. R.; Westmoreland, T. D.; Caspar, J. V.; Barqawi, K. R.; Meyer, T. J. *Inorg. Chem.* **1988**, *27*, 3195.
(15) Heath, G. A.; Smeulders, J. B. A. F. Presented at the XXVIIth International Conference on Coordination Chemistry, Broadbeach, Australia, 1989; Abstract W39. Heath, G. A.; Kennedy, B. J. To be published.
(16) Duff, C. M.; Heath, G. A.; Willis, T. C. *Acta Crystallogr.* **1990**, *C46*, 2320.

Table III. Position of the Principal LMCT and MLCT Bands in $[RuX_{6-n}(RCN)_n]^z$ Complexes (X = Cl^- and Br^-) as a Function of Stoichiometry and Oxidation State[a-f]

stoichiometry	Cl → Ru^{IV}	Cl → Ru^{III}	Ru^{II} → RCN (chlorides)	Ru^{II} → RCN (bromides)	Br → Ru^{III}	stoichiometry
$RuCl_6$[a]	20 250, 22 240	28 250, 30 980*	–	–	21 250, 25 670*	$RuBr_6$[a]
$RuCl_5(PhCN)$	20 500*	26 400*			19 750, 21 400*	$RuBr_5(PhCN)$[b]
$RuCl_5(MeCN)$	20 600*	27 000*				
$RuCl_4(PhCN)_2$[b]	17 910, 19 140*	23 720, 24 500	23 065*	22 600*	17 500, 19 600	$RuBr_4(PhCN)_2$[b]
$RuCl_4(MeCN)_2$[b,d]	17 800, 19 600*	24 250, 25 200				
$RuCl_3(PhCN)_3$		23 790	25 690*	26 100*	18 000*	$RuBr_3(PhCN)_3$
$RuCl_3(MeCN)_3$[d]	20 200*	24 800				
$RuCl_2(PhCN)_4$		21 460*	29 270	30 500	15 700*	$RuBr_2(PhCN)_4$
$RuCl(PhCN)_5$		19 100*	33 200	33 300		$RuBr(PhCN)_5$
$Ru(PhCN)_6$	–	–	36 230	36 230	–	$Ru(PhCN)_6$

[a] For the hexahalides, the mean of the T_{1u} and T_{2u} transition energies is used in frequency vs stoichiometry correlations. [b] The double entries refer to halide-based spin–orbit splitting of the orbitally degenerate transition. [c] Data indicated by asterisks were obtained by in situ spectroelectrogeneration, conditions as given in Table I unless otherwise noted; data without asterisks refer to stable compounds measured under Ar in CH_2Cl_2 at 20 °C. [d] Spectroelectrochemical generation in 0.1 Bu_4NBF_4/CH_3CN at −35 °C. [e] Extensive observations confirm that these data are unchanged by the presence of electrolyte or nitrile, or varying temperatures, providing stability is maintained. [f] For X → Ru^{III} bands,[3] the assigned transition symmetries are as follows: $n = 0$, T_{1u} and T_{2u}; $n = 1$, E; $n = 2$, E_u; $n = 3$, A_1; $n = 4$, E_u; $n = 5$, E.

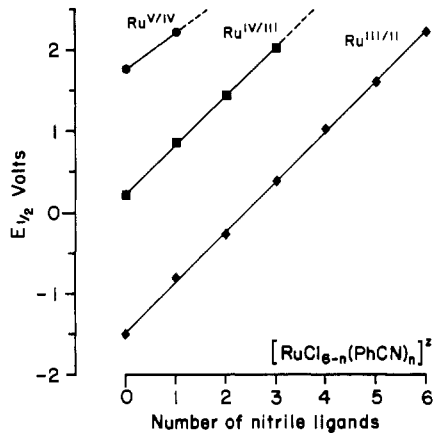

Figure 1. Electrode potentials of the series $[RuCl_{6-n}(PhCN)_n]^{z/z-1}$ as a function of stoichiometry: correlation of $E_{1/2}(Ru^{V/IV})$ (●), $E_{1/2}(Ru^{IV/III})$ (■), and $E_{1/2}(Ru^{III/II})$ (♦) with the number of nitrile ligands (n). The electrode potential data are listed in Table I; the least-squares fitted gradients are found in Table II.

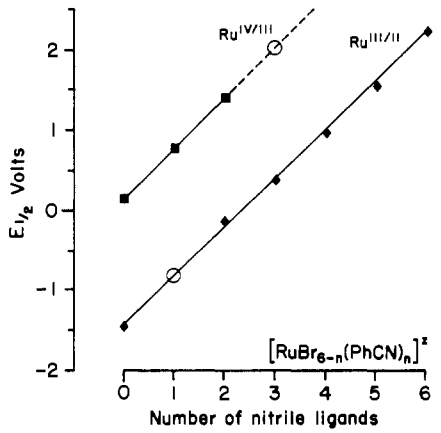

Figure 2. Electrode potentials of the series $[RuBr_{6-n}(PhCN)_n]^{z/z-1}$ as a function of stoichiometry: correlation of $E_{1/2}(Ru^{IV/III})$ (■) and $E_{1/2}(Ru^{III/II})$ (♦) with the number of nitrile ligands (n). The electrode potential data are listed in Table I; the least-squares fitted gradients are found in Table II. $E_{1/2}(Ru^{III/II})$ for $[RuBr_5(PhCN)]^{2-/3-}$ is predicted to be −0.83 V, and $E_{1/2}(Ru^{IV/III})$ for $[RuBr_3(PhCN)_3]^{+1/0}$ is predicted to be +2.05 V.

All couples showed reversible voltammetric response under the conditions given in Table I, except for $[RuX_5(RCN)]^{2-/3-}$ and $[RuX_6]^{3-/4-}$. A wealth of redox-linked substitution chemistry arises when temperatures are higher or the concentration of nitrile greater than specified in Table I, but this subject is taken up separately.[3]

Our primary objective here is to reliably define the relative electrode potentials within the $RuX_{6-n}(RCN)_n$ family, even though the conditions necessary to achieve reversibility for the various couples differ widely and are frequently mutually incompatible. Therefore all measurements in Table I are cross-referenced to one or both of two accessible internal standards, $[RuX_6]^{2-/3-}$ and $[RuX_4(RCN)_2]^{1-/2-}$ (X = Cl^- or Br^-, as appropriate), which are set at their CH_2Cl_2/−70 °C values (vs Ag/AgCl). Determined in this way, the values listed are mutually consistent within 30 mV and agree with independent measurements made with ferrocene as an internal reference.

The general trend of the three accessible electrode potentials ($Ru^{V/IV}$, $Ru^{IV/III}$, $Ru^{III/II}$) with varying stoichiometry is illustrated in Figures 1 and 2. Least-mean-squares treatment of the data confirms close linear correlations between the $E_{1/2}$ values and the extent of halide ligation ($6-n$), as detailed below.

$[RuCl_{6-n}(PhCN)_n]^z$ Data (Figure 1). The $E_{1/2}(Ru^{III/II})$ values for $n = 0$–6 define a line of gradient +0.62 V/chloride lost (V/Cl^-), with a correlation coefficient (r) of 0.999. Similarly, $E_{1/2}(Ru^{IV/III})$ values for $n = 0$–3 vary by +0.60 V/Cl^- with r = 1.000. $E_{1/2}(Ru^{V/IV})$ shifts by +0.45 V/Cl^- between $[RuCl_6]^{2-}$ and $[RuCl_5(PhCN)]^-$.

$[RuBr_{6-n}(PhCN)_n]^z$ Data (Figure 2). The $E_{1/2}(Ru^{III/II})$ values for $n = 0$–6 vary by +0.59 V/Br^- with r = 0.998. The $E_{1/2}(Ru^{IV/III})$ values for $n = 0$–2 vary by +0.64 V/Br^- with r = 1.000. The $Ru^{IV/III}$ couple of $[RuBr_3(PhCN)_3]$ is unobservable due to the intervening destructive oxidation of bromide.[3]

$[RuCl_{6-n}(MeCN)_n]^z$ Data. The $E_{1/2}$ values for this series were determined for $n = 0$–4. The $Ru^{III/II}$ couple shifts by +0.59 V/Cl^- with r = 0.999, and the $Ru^{IV/III}$ couple shifts by +0.57 V/Cl^- with r = 0.995. In addition, $E_{1/2}(Ru^{V/IV})$ shifts by +0.42 V/Cl^- between $[RuCl_6]^{2-}$ and $[RuCl_5(MeCN)]^-$.

Charge-Transfer Spectra. The electronic absorption spectra were recorded in the range 45 000–10 000 cm^{-1}. Principal charge-transfer bands are listed in Table III. For the oxidized and reduced species, initially detected by the reversible voltammetric response of their parent compounds, the optical spectra were obtained by in situ generation in a spectroelectrochemical cell. This technique has enabled us to characterize 17 otherwise inaccessible species: $[Ru^{IV}Cl_{6-n}(PhCN)_n]^{n-2}$, n = 1–3; $[Ru^{IV}Cl_{6-n}(MeCN)_n]^{n-2}$, n = 1–3; $[Ru^{III}Cl_{6-n}(PhCN)_n]^{n-3}$, n = 1, 4, 5; $[Ru^{III}Br_{6-n}(PhCN)_n]^{n-3}$, n = 1, 3, 4; $[Ru^{II}Cl_{6-n}(PhCN)_n]^{n-4}$, n = 2, 3; $[Ru^{II}Br_{6-n}(PhCN)_n]^{n-4}$, n = 1–3.

A typical experiment is illustrated in Figure 3, which shows the anodic generation of $[Ru^{IV}Cl_3(MeCN)_3]^+$ from $[Ru^{III}Cl_3(MeCN)_3]$ at −35 °C and +2.1 V. The maintenance of strict isosbestic points in successive spectra strongly suggests the presence of a single product throughout the course of the electrolysis.[12a] When electrogeneration is complete, the product should be returned to the initial state by application of the appropriate potential, in order to verify the chemical reversibility of the process through full recovery of the original spectrum (as in the present

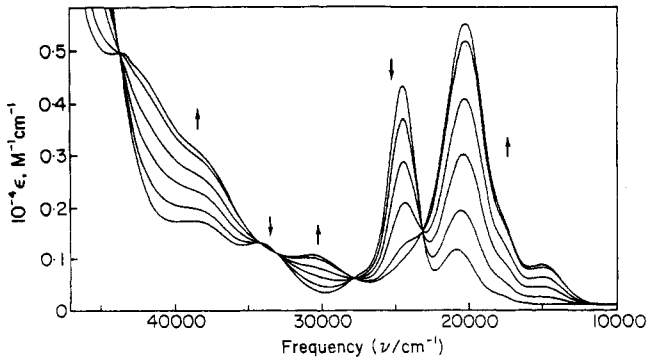

Figure 3. Spectral progression accompanying anodic electrogeneration of $[RuCl_3(CH_3CN)_3]^+$, at −35 °C and +2.1 V, from $[RuCl_3(CH_3CN)_3]$ (5×10^{-3} M) in CH_3CN containing Bu_4NBF_4 (0.1 M). Arrows indicate the direction of change.

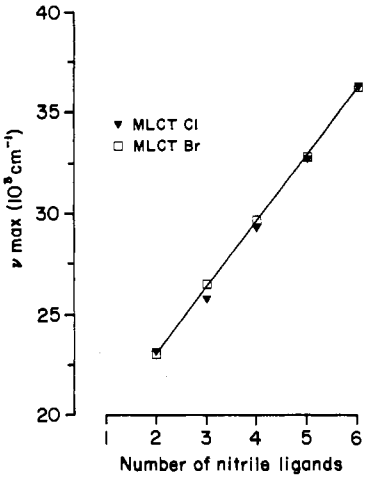

Figure 4. Ruthenium(II) to nitrile charge-transfer band energy as a function of stoichiometry. Band maxima (Table III) are plotted vs n for $[RuX_{6-n}(PhCN)_n]^{4-n}$: X = Cl (▼) and X = Br (□).

example). These stringent criteria have been applied throughout this work. For a reactive compound, the technique permits a high level of confidence in all features of the spectrum because of their progressive and reversible development.

The requirements for successful reversible electrogeneration are intrinsically more challenging than for voltammetry, because the reactive species should retain complete integrity over a time scale of minutes or even hours rather than milliseconds. This brings the electrogenerated compound into the realm of normal chemical stability. For example, there may be a need for additional free ligand to inhibit loss of coordinated L or lower temperatures to inhibit incorporation of further L or even a difficult balance between these contrary problems, bearing in mind that the stability of the complex in two oxidation states is simultaneously at issue. As far as possible, the reversible voltammetric conditions presented for individual systems in Table I were chosen to match the requirements for chemically reversible spectroelectrochemistry as well.

The charge-transfer spectra of the Ru^{II} complexes are all relatively simple and permit ready analysis, since they exhibit one strong MLCT ($Ru^{II} \rightarrow RCN$) band. This band shifts systematically to higher energy as the series progresses from $[RuX_4(PhCN)_2]^{2-}$ to $[Ru(PhCN)_6]^{2+}$ (Figure 4). Mean shifts per halide replaced of 3350 cm^{-1} for X = Cl$^-$ (r = 0.997) and 3300 cm^{-1} for X = Br$^-$ (r = 1.00) were determined by least-squares treatment of the data.

At the Ru^{III} level, the LMCT ($X^- \rightarrow Ru^{III}$) bands shift to lower energy across the complete series, $[RuX_6]^{3-}$ to $[RuX(RCN)_5]^{2+}$, although there is clearly a deviation between n = 2 and n = 3. Figure 5 shows the energy of the dominant LMCT band plotted against the extent of halide ligation (6−n). Overall gradients of −1930 cm^{-1}/Cl$^-$ (r = 0.96) for $[Ru^{III}Cl_{6-n}(PhCN)_n]^{n-3}$, −1800

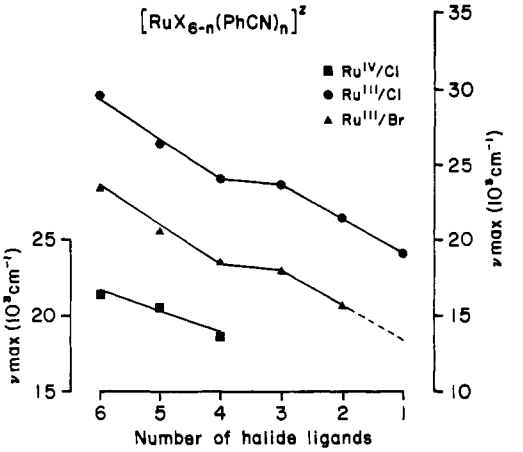

Figure 5. Halide to ruthenium charge-transfer band energy as a function of stoichiometry. The optical data (Table III) are plotted against the number of halide ligands (6−n) for $[RuX_{6-n}(PhCN)_n]^z$: Cl$^- \rightarrow Ru^{III}$ (●), Br$^- \rightarrow Ru^{III}$ (▲), and Cl$^- \rightarrow Ru^{IV}$ (■). Data for the Ru^{IV}/Cl$^-$ series are displaced by 5000 cm^{-1}, as shown.

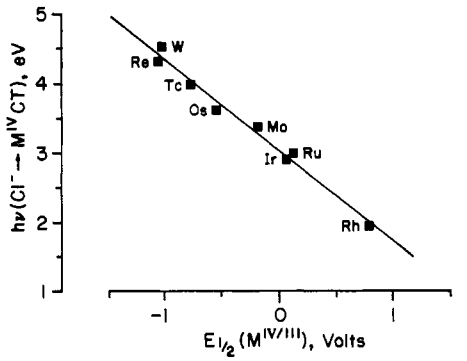

Figure 6. Correlation of central ion reduction potentials and chloride-to-metal charge-transfer band energies for a series of 4d^n and 5d^n $[MCl_6]^{2-}$ complexes ($n \leq 5$): Electrochemical data, $E_{1/2}(M^{IV/III})$, are drawn from ref 2; optical data π-$t_{2u}(Cl^-) \rightarrow t_{2g}(M^{IV})$ are from Table 5.6 of Lever's text.[12] The line has a gradient of 1.31 eV/V with a correlation of r = 0.983.

cm^{-1}/Br$^-$ (r = 0.96) for $[Ru^{III}Br_{6-n}(PhCN)_n]^{n-3}$, and −1800 cm^{-1}/Cl$^-$ (r = 0.95) for $[Ru^{III}Cl_{6-n}(MeCN)_n]^{n-3}$ (not included in Figure 5) were calculated from least-mean-squares analysis. Separate analysis of the two distinct segments of each PhCN plot gives gradients of 2760 and 2350 cm^{-1}/Cl$^-$ and of 2425 and 2300 cm^{-1}/Br$^-$, for the first (n = 0–2) and second (n = 3–5) segments, respectively.

For a given stoichiometry, the LMCT spectra of the Ru^{IV} and Ru^{III} states are similar in general appearance, as for example in Figure 3. The Ru^{IV} LMCT bands shift steadily to lower energy from $[RuCl_6]^{2-}$ to $[RuCl_4(RCN)_2]$. Analysis of the most intense LMCT band as a function of halide ligation (6−n) yields gradients of −1640 cm^{-1}/Cl$^-$ with r = 0.99 for PhCN/Cl$^-$ substitution (Figure 5) and −1350 cm^{-1}/Cl$^-$ with r = 0.92 for MeCN/Cl$^-$ where n = 0–2. The band actually moves to higher energy for $[RuCl_3(MeCN)_3]^+$ (Table III), emphasizing the tendency noted above for the LMCT progression to be interrupted at this point.

Finally, looking more widely across the 4d and 5d elements, the acquisition of comprehensive electrode potential data for the hexachlorometalates (M = Zr to Pd and Hf to Pt)[1,2] has made it possible to examine the correlation of halide to metal charge-transfer band energies with the appropriate central ion reduction potential. The hexahalide spectra are characteristically complex but well understood, with comparable Cl$^-$(π) to M(dπ) transitions readily identified in each case. Figure 6 presents the linear correlation between $E_{1/2}(M^{IV/III})$ and ν_{max}, for Cl$^-$(t_{2u}) $\rightarrow M^{IV}(t_{2g})$ promotion, for all accessible $[MCl_6]^{2-}$ complexes. As recently reported,[15] a parallel $h\nu$ vs $E_{1/2}$ relationship exists for the numerous 4d and 5d hexahalides in oxidation state V, as well as for the smaller number of M^{III} complexes with a vacancy in the t_{2g} subshell

Scheme I

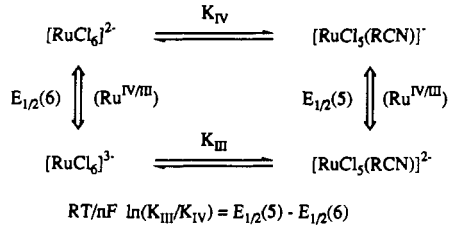

$$RT/nF\ \ln(K_{III}/K_{IV}) = E_{1/2}(5) - E_{1/2}(6)$$

to permit $\pi \rightarrow d\pi$ charge transfer.

Discussion

Voltammetry. The exact linearity of the $E_{1/2}$ values as a function of stoichiometry within the present $[RuX_{6-n}(RCN)_n]^z$ series is striking (Figures 1 and 2). The consequences of differing molecular geometry are evidently minimal in these compounds, and the electrode potentials of the alternative *cis*-X_4, *fac*-X_3, and *cis*-X_2 isomers are not expected to differ significantly from the trends shown in Figures 1 and 2. For example, on AOM considerations[6] and on general structural grounds, it is *mer*-$[RuX_3(RCN)_3]$ rather than the absent *fac* isomer which should show any deviation of $E_{1/2}(Ru^{III/II})$ from the mean of $[RuX_6]^{3-}$ and $[Ru(RCN)_6]^{3+}$. Theoretically, the divergence of $E_{1/2}$ values for isomeric complexes should increase with the difference in π-bonding character within the ligand array.[8,9] The selection of nitrile as a representative neutral ligand in the present study was partly suggested by its modest π-bonding properties.

As seen in Table II, the difference in gradient between the acetonitrile and benzonitrile series is small but consistent for the V/IV, IV/III, and III/II couples (0.03 V/Cl^- steeper for PhCN than for MeCN in each case). The $E_{1/2}$ data for corresponding chloro and bromo complexes are also very close, not only in gradient but in absolute value. These observations can be compared with the shift in the $Ru^{III/II}$ couple upon halide/nitrile replacement at a $Ru(bpy)_2$ binding site suggested by the Chatt–Datta analysis,[5,7] where $\Delta P_L\beta = 0.65 \pm 0.05$ V for PhCN/Cl and 0.52 ± 0.05 V for MeCN/Cl.

In thermodynamic terms, the shift of 0.6 V in electrode potential we observe between substitutionally related complexes, for example between $[RuCl_6]^{2-/3-}$ and $[RuCl_5(RCN)]^{-/2-}$, means that one-electron reduction of the metal center promotes the halide-displacement equilibrium linking the two stoichiometries by an estimated factor of 10^{10} at room temperature (see Scheme I). The linear progression of the $Ru^{IV/III}$ electrode potentials shows that this very large promotion factor is essentially constant from the first to the last displacement of halide by nitrile. Furthermore, in this study the $Ru^{IV/III}$ and $Ru^{III/II}$ couples vary in a parallel manner, implying that the associated halide/nitrile substitution equilibria are shifted by the same factor upon reduction of Ru^{III} to Ru^{II}. This simple equality may conceal underlying complexities, since the shift for the available $Ru^{V/IV}$ couples is significantly less (0.45 V).

Nevertheless, as shown in Figures 1 and 2, the separation between $Ru^{IV/III}$ and $Ru^{III/II}$ couples is essentially constant at $\sim$1.6 V in complexes ranging in composition from RuX_6 to $RuX_3(RCN)_3$ and possibly to $Ru(RCN)_6$. There is some justification for this extrapolation to $n = 6$; although $Ru^{IV/III}$ is unobservable for $n > 3$, the $Ru^{III/II}$ line shows no deviation thoughout the range. As has been demonstrated for the parent hexahalide complexes,[1,2] the separation between successive redox couples of a given metal ion directly reflects interelectronic correlations within the t_{2g} subshell.

$$[Ru^{IV}] + [Ru^{II}] \rightarrow [Ru^{III}] + [Ru^{III}]$$
$$d^4 \quad d^6 \quad d^5 \quad d^5$$

For this favored electronic redistribution between low-spin complexes of the same stoichiometry, the term $[E_{1/2}(Ru^{IV/III}) - E_{1/2}(Ru^{III/II})]$ directly reflects the sum of the prevailing repulsion and exchange energies, expressible in Racah integrals as $\{A - 5B\}$.[1] In the present context, the electrochemical data suggest that even wholesale replacement of chloride by nitrile does not cause a measurable nephelauxetic reduction of π-electron density at the metal. This is a surprising proposition given the apparent complementary nature of halide and organonitrile as potential π-donor and π-acceptor ligands, respectively. It is clearly related to our observation that electrode potentials of ruthenium binary halide/nitrile complexes are not sensitive to structural isomerization, another situation where differential π-bonding should come to the fore. Bursten also finds the latter phenomenon "nonintuitive".[8]

Table II summarizes experimentally determined quantitative trends for all these nitrile-substituted metal halide complexes. The present findings are in accord with preliminary studies on $[OsBr_{6-n}(RCN)_n]^z$ where, on substitution of nitrile for bromide, the IV/III couples shift by 0.58 V while the V/IV couples shift by 0.43 V.[17] It is remarkable that the sensitivity of the reduction potentials to ligand substitution is consistent for 4d and 5d metals (Ru and Os; Nb and Ta) and across the d block (group 5 and group 8 metals). For the various families of nitrile-substituted transition-metal complexes so far examined, the characteristic shift in reduction potentials appears to depend only on the oxidation state of the metal ion.

Correlation with Ligand Electrochemical Parameters. In this section we discuss the relationship between voltammetric aspects of the present investigation, i.e., the extended set of measured electrode potentials for $[RuX_{6-n}(RCN)_n]^z$ complexes, and Lever's recent wide-ranging study of ligand additivity.[11] A new ligand-specific electrochemical parameter, E_L, was established by analyzing the additive influence of 2,2′-bipyridyl and accompanying ligands (L) on the documented $Ru^{III/II}$ couples of over 300 $Ru(bpy)_2L_2$ and $Ru(bpy)L_4$ complexes in acetonitrile. The data base was then further enlarged by consideration of α-diimines other than bpy itself. In this fashion values for many ligands have been estimated, including Br^-, Cl^-, MeCN, and PhCN. In principle the electrode potential for any new permutation can be predicted by summing over the appropriate ligand array. E_L is defined such that the relationship below is satisfied for each six-coordinate complex in the data set, where the intercept is expected to be zero when potentials are expressed vs the NHE and the least-squares-fitted gradient is expected to be one (for $Ru^{III/II}$ couples).

$$E_{1/2}(Ru^{III/II}) = m\sum E_L + b$$

Inspection shows that the data base of ref 11 is rich in acetonitrile and chloride compounds; however there are no more than two X^- or RCN ligands in any tabulated complex, and mixed halide/nitrile compounds are virtually unrepresented in the assignment of E_L values. Clearly, our measurements of $E_{1/2}(Ru^{III/II})$ spanning all seven possible stoichiometries of simple binary halide/nitrile complexes provide a significant test of Lever's model. Impressively, the shifts estimated from $\sum E_L$ for replacement of Cl^- by PhCN or MeCN and of Br^- by PhCN turn out to coincide within 10 mV with the accurately defined experimental gradients (Table II). Plotting $E_{1/2}(Ru^{III/II})$ (Table I) against $\sum E_L$ yields the following equation for the line of best fit:

$$E_{1/2}(Ru^{III/II}) = 1.01\sum E_L - 0.063$$
$$r = 0.999,\ 17 \text{ complexes}$$

Incidentally, the observed intercept constitutes a good, statistically averaged estimate of the numerical relationship between $Ru^{III/II}$ couples measured under our conditions and standard measurements in CH_3CN vs the NHE (see Table I).

Lever noted that few data sets exist for different oxidation states of the same metal ion and that no appropriate ones were available for $Ru^{IV/III}$. Our investigation redresses this in an ideal way, by examining the accessible $Ru^{IV/III}$ couples as well as the $Ru^{III/II}$ couples for the same compounds. This means that the corresponding relationship between $E_{1/2}(Ru^{IV/III})$ and $\sum E_L$ can also be analyzed:

$$E_{1/2}(Ru^{IV/III}) = 1.01\sum E_L + 1.523$$
$$r = 0.984,\ 11 \text{ complexes}$$

(17) Duff, C. M.; Heath, G. A.; Kang, Y. B. Unpublished results.

The good fit and unaltered slope, illustrating the application of $\sum E_L$ values in this new context, both follow naturally from the observation of parallel variation in $Ru^{IV/III}$ and $Ru^{III/II}$ couples with stoichiometry in $[RuX_{6-n}(RCN)_n]^z$. Equally, the difference in intercept in the two $\sum E_L$ plots reflects the characteristic separation between $Ru^{III/II}$ and $Ru^{IV/III}$ couples, which has been discussed above (cf. Figures 1 and 2).

Charge-Transfer Spectra. As evident from the earlier discussion, placing an increasing number of halide ligands around the metal center effectively raises the energy of the d orbitals. Qualitatively, therefore, this should be associated with a progressive red shift of the metal to ligand charge transfer ($Ru^{II}(d\pi) \rightarrow RCN(\pi^*)$) and a corresponding blue shift of ligand to metal charge transfer ($X^-(p\pi) \rightarrow Ru^{III}(d\pi)$ and $X^-(p\pi) \rightarrow Ru^{IV}(d\pi)$). This expectation is modified by recognizing that the introduction of the negative ligands must also destabilize the neighboring ligand orbitals to an uncertain extent.

The anticipated correlation between optical charge-transfer energy and the extent of halide ligation is amply demonstrated by the behavior of the Ru^{II} to nitrile MLCT bands. Within the series $[RuX_{6-n}(PhCN)_n]^z$ (n = 2–6, X = Cl^- and Br^-) the MLCT band position is strongly dependent on stoichiometry and is independent of the identity of the halide (Figure 4). The linearity of the correlation is surprisingly robust since it is evidently indifferent to the variations in molecular symmetry, overall charge, and polarity.

The halide to Ru^{III} charge-transfer manifold is more complex in appearance than the Ru^{II} to nitrile charge-transfer manifold and exhibits greater qualitative variation through the series. However, the most prominent absorption arises from a physically analogous orbitally allowed in-plane transition in each case (n = 0–5), despite the changes in structure and symmetry.[3,18] Overall, the Ru^{III} LMCT band energies follow trends with stoichiometry which are complementary to the behavior described above for MLCT spectra. The LMCT bands of the Ru^{III} bromo series mirror those of the chloro series in appearance although increased splitting due to halide-centered spin–orbit coupling is evident in the doubly degenerate main band of $[RuBr_5(RCN)]^{2-}$ and $[RuBr_4(RCN)_2]^-$. The chloro and bromo plots in Figure 6 are separated by an average of 6000 cm^{-1}, in accord with the easier oxidation of bromide. Thus, in sharp contrast to the Ru^{II} to nitrile transitions, the LMCT spectra are sensitive to the identity of the halide which is now integral to the chromophore.

We associate the very noticeable deviation in the plots between n = 2 and 3 with the first removal of a halide ion from within the characteristic planar MX_4 chromophore. This leads to pronounced stabilization of the donor levels of the remaining halide ligands with a consequent increase in charge-transfer energy. Both covalent halide/halide interactions and the opportunity for extensive mixing of $\pi(X^-)$ with $\sigma(X^-$ or RCN) levels in *mer*-MX_3L_3 complexes under C_{2v} symmetry should be considered.[3] However, a ready explanation is provided simply by the decrease in mutual X^-/X^- electrostatic repulsions within the MX_3 chromophore.

Spectral data at the Ru^{IV} level are limited to three complexes of the benzonitrile–chloro family and four of the acetonitrile–chloro family. Truncation of this series curtails investigation of the variation of the Ru^{IV} band energy with stoichiometry. However for the complexes with n = 0–2 there is a consistent progression of the LMCT bands to lower energy. These effects greatly exceed the modest concerted changes noted in optical spectra and $E_{1/2}(M^{IV/III})$ for tetravalent $[OsX_4L_2]$ and $[IrX_4L_2]$ compounds when only the identity of the neutral ligand varies (L = PR_3, AsR_3).[19]

Frontier Orbital Mapping. Thus far we have deliberately presented systematic relationships which are purely empirical, for example plotting electrode potentials or optical transition energies versus stoichiometry. However, it is instructive to merge these electrochemical and spectroscopic observations into one conceptual framework. We can ascribe notional redox potentials ($E^*_{1/2}$) to the nitrile acceptor and halide donor, and so express the charge-transfer transition energies as follows.

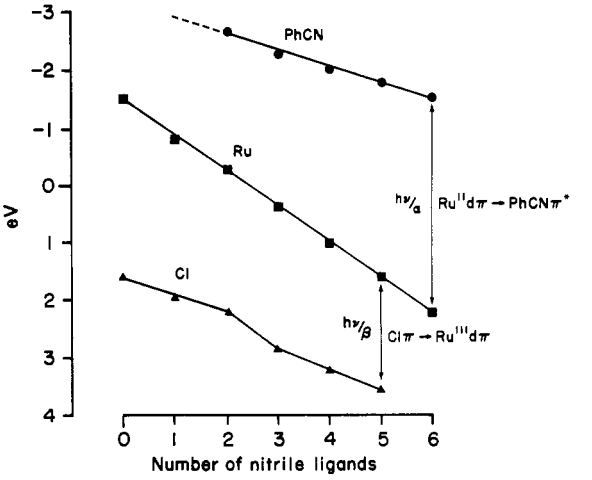

Figure 7. Behavior of the frontier orbital domain in ruthenium chlorobenzonitrile complexes: the movement of $E_{1/2}(Ru^{III/II})$ (■), $E^*_{1/2}(Cl^{0/1-})$ (▲), and $E^*_{1/2}(PhCN^{0/1-})$ (●) as a function of stoichiometry (constructed by use of eqs 1 and 2, setting $\alpha = \beta = 1.2$).

MLCT:

$$h\nu(Ru^{II} \rightarrow RCN) = \alpha[E_{1/2}(Ru^{III/II}) - E^*_{1/2}(RCN^{0/-})] \quad (1)$$

LMCT:

$$h\nu(X^- \rightarrow Ru^{III}) = \beta[E^*_{1/2}(X^{0/-}) - E_{1/2}(Ru^{III/II})] \quad (2)$$

These equations are in accord with the wide-spread empirical observation of linear relationships between charge-transfer band energies and electrochemical potentials, and they have a firm theoretical foundation as explained below. The spectroelectrochemical proportionality factor (α or β) has been found to be constant in a given chemical context. For example, we observe a value of 1.31 for LMCT in $[MCl_6]^{2-}$ systems, taking $E^*_{1/2}(Cl^{0/-})$ to be invariant within that family (Figure 6), and Meyer found 1.16 for MLCT excitation in numerous osmium(II) diimine systems.[14] This factor is typically somewhat greater than unity in accord with the intrinsic additional energization of the nonequilibrated optically excited states.[13,14]

Figure 7 shows the trend in frontier orbital relationships between metal and ligands for the $[RuCl_{6-n}(PhCN)_n]^z$ family, constructed by use of eqs 1 and 2. Note that the vertical axis is related to electrode potential; i.e. these data are electron-transfer couples, not orbital energies, and as such they are particularly appropriate for describing both redox and optical charge-transfer phenomena. For example, the metal-centered electron/electron correlation terms, which require explicit estimation in other treatments,[20] are automatically encompassed in experimental $E_{1/2}$ values.

If there were no change in the overall energy of the halide or nitrile orbitals upon progressive substitution, the rate of change of the charge-transfer transition energies would match that of the metal-based electrode potentials. By contrast, in circumstances where replacement of halide by a neutral ligand stabilizes the metal and ligand orbitals to the same extent, the charge-transfer bands will not shift with varying stoichiometry. The Jorgenson optical electronegativity model is equally restrictive since, in a specified oxidation state, neither metal nor ligand X_{opt} is considered to vary.[20]

For the binary halide/nitrile complexes of ruthenium studied here, it is clear that none of these models is adequate; replacement of each chloride by benzonitrile stabilizes the ruthenium orbitals to the greatest degree (0.62 eV), affects the π-donor levels of the remaining coordinated chlorides to a smaller extent (0.40 eV overall mean), and lowers the nitrile π-acceptor orbitals still less (0.28 eV). This may be compared with theoretical estimates of 0.25–0.5 eV for halide/halide interactions in *cis*-$[RuX_2(NH_3)_4]^+$ (X = Cl^- or Br^-).[18]

(18) Verdonck, E.; Vanquickenborne, L. G. *Inorg. Chem.* **1974**, *13*, 762.
(19) Cipriano, R. A.; Levason, W.; Mould, R. A. S.; Pletcher, D.; Webster, M. *J. Chem. Soc., Dalton Trans.* **1990**, 339.
(20) Jorgenson, C. K. *Prog. Inorg. Chem.* **1970**, *12*, 101.

It is interesting to note that in the $OsX_{6-n}(NH_3)_n$ family (X = Cl^-, Br^-, I^-; n = 2–4), where the measured change in the $Os^{IV/III}$ couple is 0.33 V/X^- rather than 0.6 V/X^-, the halide to metal charge-transfer bands do not shift appreciably as the stoichiometry alters.[21] Clearly, this is well accommodated by our model. A diagram for $OsX_{6-n}(NH_3)_n$ constructed similarly to Figure 7 shows the metal- and halide-based couples declining at the same rate.

In the mixed nitrile compounds, the characteristic shifts in frontier orbitals upon ligand substitution represent the summation of covalent and electrostatic effects of halide loss and nitrile addition. While these contributions cannot be experimentally partitioned, we stress that each introduction of a closed-shell negative-ion significantly destabilizes the neighboring halide and benzonitrile ligands. Thus, in addition to the familiar effects of the ligands on the metal center, a "ligand field theory for ligands" is required. The present analysis is an early step in the quantification of these terms. For example, Figure 7 emphasizes that the distinct deviation observed between MX_4 and MX_3 chromophores in the Ru^{III} LMCT plot (Figure 5) arises specifically from additional stabilization of the halide donor orbitals in $RuCl_3(PhCN)_3$, as discussed above.

Conclusions

In complexes of general form $MX_{6-n}(RCN)_n$, systematic relationships have been demonstrated between the extent of halide ligation and the electrode potentials characterizing the coordinated metal ion. The same dependence of $E_{1/2}$ on n is found for both chloride and bromide, is common to congeneric $4d^n$ and $5d^n$ metal ions, and is shared by isovalent metal ions as diverse as niobium and ruthenium.

As noted in the introduction, one corollary of such wide-ranging ligand-additivity relationships is that any family of complexes where the stoichiometry is fixed and the metal varies widely should show extended periodic patterns in electrode potentials.[1,2] For the hexahalometalates themselves, the optical halide to metal charge-transfer energies are now shown to systematically reflect the corresponding central ion reduction potentials. The spectra then provide an equivalent periodic expression of the underlying progressions in core charge, electronic correlation terms, and relativistic effects.

The study of the $RuX_{6-n}(RCN)_n$ systems has included investigation of their accessible $Cl \rightarrow Ru^{IV}$, $Cl \rightarrow Ru^{III}$, and $Ru^{II} \rightarrow RCN$ charge-transfer bands. These spectra also follow trends fully complementary to the orderly trends in the appropriate central ion electrode potential, once the accompanying variations in halide and nitrile frontier orbitals are taken into account. This approach offers an integrated empirical analysis of charge-transfer spectra, quantified by electrochemical measurements on the complexes concerned rather than by appeal to generalized optical electronegativity parameters. Finally, as made clear in the Discussion, we stress that the very orderly empirical behavior presented here, characterized by linear progressions in both $E_{1/2}$ and charge-transfer energy, will not necessarily prevail in chemically dissimilar systems.

Appendix: Derivation of Equations 1 and 2

The most general statement of the empirical behavior we observe would be

$$h\nu \text{ (in eV)} = \alpha\Delta E_{1/2} + \text{constant} \quad (3)$$

In the present treatment such a constant, if non-zero, will simply be concealed in $E^*_{1/2}$, the value assigned to the electrode potential of the ligand, and has no bearing on our current conclusions. However, an explicit constant is not required in the development of eqs 1 and 2 from first principles, as set out below.

It is necessary to define the half-cell reactions relevant to metal to ligand charge-transfer processes in solution. Representing the ground-state complex as [M-L] and visualizing the stable oxidized and reduced forms as $[M^+\text{-}L]^+$ and $[M\text{-}L^-]^-$ and the equilibrated MLCT excited state as $[M^+\text{-}L^-]^*$, we have

a $\quad [M^+\text{-}L]^+ + e^- \rightarrow [M\text{-}L] \quad E_{1/2}(M^+/M)$

b $\quad [M\text{-}L] + e^- \rightarrow [M\text{-}L^-]^- \quad E_{1/2}(L/L^-)$

c $\quad [M^+\text{-}L]^+ + e^- \rightarrow [M^+\text{-}L^-]^* \quad E^*_{1/2}(L/L^-)$

The discussion between eqs b and c is that in the latter, voltammetrically unmeasurable process, the ligand is reduced in the presence of the oxidized metal ion.

We can now combine half-cells and specify $\Delta G°$ for the following thermally equilibrated solutions processes, setting $\Delta E_{1/2}$ equal to minus the standard cell potential to avoid intrusion of negative signs.

(c - a) excitation:

$$[M^+\text{-}L]^+ + [M\text{-}L] \xrightarrow{a} [M\text{-}L]^+ + [M\text{-}L]^* \qquad \Delta E_{1/2}(\text{excitn})$$

(b - a) disproportionation:

$$[M\text{-}L] + [M\text{-}L] \xrightarrow{a} [M\text{-}L]^+ + [M\text{-}L]^- \qquad \Delta E_{1/2}(\text{dispro})$$

(c - b) promotion by comproportionation:

$$[M\text{-}L]^+ + [M\text{-}L]^- \xrightarrow{b} [M\text{-}L] + [M\text{-}L]^* \qquad \Delta E_{1/2}(\text{compro})$$

For the excitation reaction, the term $\Delta E_{1/2}$(excitn) is equivalent to the term $[E_{1/2}(Ru^{III/II}) - E^*_{1/2}(RCN^{0/-})]$ in eq 1 of the main text. Naturally, a corresponding set of electrode couples and cell reactions exists dealing with ligand to metal charge transfer. In correlating redox and optical charge-transfer behavior, there has been a tendency elsewhere to focus on $\Delta E_{1/2}$(dispro) rather than $\Delta E_{1/2}$(excitn), especially for the bipyridyl systems, prompted by the availability of both $E_{1/2}(M^+/M)$ and $E_{1/2}(L/L^-)$ data. Reaction c–b measures the difference between disproportionation and the true excitation reaction.

We take as our starting point eq 4, the relationship advanced by several authorities,[22-26] where E_o and ΔG refer respectively to the internal energy and free energy change in reaching the thermally equilibrated excited state from the ground state in solution.

$$h\nu = E_o + \chi \quad (4a)$$

$$h\nu = \Delta G + \lambda \quad (4b)$$

The terms χ and λ are the associated internal energy and free energy contributions arising from vibrational reorganization of the complex and its solvent cage. The Franck–Condon excitation energy, $h\nu$, is itself entropy neutral and may be treated interchangeably as a free energy or internal energy term. Meyer has developed eq 4a in detail.[22] He stresses that complexities are introduced in replacing the internal energy term E_o by measurable metal and ligand redox potentials. The necessary corrections for resonance, electrostatic, and entropy effects are documented in eq 18 of ref 22.

We choose instead to develop the free energy relationship, (4b), taking advantage of the fact that we have so defined $E^*_{1/2}(L/L^-)$ that $nF\Delta E_{1/2}$ is an exact expression for the free energy of excitation in solution (ΔG). We note that λ in (4b) is the sum of the intramolecular (λ_i) and solvent dipole (λ_o) contributions, and that both λ_i and λ_o are themselves proportional to the energy gap between the excited state and ground state.[14,25]

To describe charge-transfer and intervalence transitions in which the electron is largely localized in initial and final states, Hush defines a vibronic coupling constant ρ such that $\chi = \rho E_0$ and $h\nu = (1 + \rho)E_0$ (eq 18 of ref 26). Likewise, setting $\lambda = \rho\Delta G$ in eq

(21) Buhr, J. D.; Winkler, J. R.; Taube, H. *Inorg. Chem.* **1980**, *19*, 2416.

(22) Curtis, J. C.; Sullivan, B. P.; Meyer, T. J. *Inorg. Chem.* **1983**, *22*, 224.
(23) Dodsworth, E. S.; Lever, A. B. P. *Chem. Phys. Lett.* **1984**, *112*, 567.
(24) Marcus, R. A. *J. Chem. Phys.* **1965**, *43*, 1261.
(25) Sullivan, B. P.; Curtis, J. C.; Kober, E. M.; Meyer, T. J. *Nouv. J. Chim.* **1980**, *4*, 643.
(26) Hush, N. S. *Electrochim. Acta* **1968**, *13*, 1005.

4b, we obtain $h\nu = (1 + \rho)\Delta G = \alpha\Delta G$, where $\alpha = (1 + \rho)$. Then, recalling $\Delta G = nF\Delta E_{1/2}$(excitn)

$$h\nu \text{ (in eV)} = \alpha\Delta E_{1/2}(\text{excitn}) \quad (5)$$

This is the physical justification for omitting an explicit constant in eqs 1 and 2.

Note that in situations outside the present context when E_0 becomes very small, as in intervalence charge transfer, ρ rises rapidly and $h\nu \gg E_0$.[26] Thus it is an abuse of the model to extrapolate the relationship to an intercept despite the excellent linearity in the present domain.

Finally, we take the opportunity to show that Lever's expression for relating $h\nu$ to measured electrode potentials (eq 4 of ref 23), though apparently more complex in form, corresponds to our starting point (eq 4b).

$$E_{op} = h\nu = [\chi_i + nF\Delta E(\text{redox}) + \Delta\Delta G_s + Q] + \chi_o + \Delta(\text{sol}) \quad (6)$$

In ref 23, χ_i and χ_o are used expressly for the *free energy* of reorganization, ΔE(redox) refers to the disproportionation reaction, and $\Delta\Delta G_s$ and Δ(sol) are solvation terms. Standardizing symbols and regrouping gives

$$h\nu = [nF\Delta E_{1/2}(\text{dispro}) + Q + \sum\Delta G_{solv}(ML_g^{*} + ML_g^{0} - ML_g^{+} - ML_g^{-})] + \lambda_i + \lambda_o \quad (7)$$

However Q is the "gas-phase resonance energy", so that $[Q + \sum\Delta G_{solv}]$ equals $nF\Delta E_{1/2}$(compro). Thus, eq 7 is equivalent to

$$h\nu = nF[\Delta E_{1/2}(\text{dispro}) + \Delta E_{1/2}(\text{compro})] + \lambda_i + \lambda_o \quad (8)$$

The sum of the disproportionation and comproportionation/promotion reactions in solution is the excitation reaction, (c-a), above, so eq 6 is fully equivalent to eq 4b.

Supplementary Material Available: Tables of analytical data and data for Figures 5 and 6 (2 pages). Ordering information is given on any current masthead page.

Contribution from the Department of Chemistry, Rutgers, The State University of New Jersey, New Brunswick, New Jersey 08903, and Department of Physics, The Hebrew University, Jerusalem, Israel 91904

Evidence for Intermediate ($S = 1$) Spin State Stabilization in $Fe^{II}(4,4'\text{-dpb})_2(NCS)_2$ and $Fe^{II}(4,4'\text{-dpb})_2(NCSe)_2$ (dpb = Diphenyl-2,2'-bipyridyl) from Susceptibility, Infrared, and ^{57}Fe Mossbauer Data

D. C. Figg, R. H. Herber,* and I. Felner

Received June 12, 1990

Magnetic susceptibility, ^{57}Fe Mossbauer spectroscopy, and variable-temperature FTIR spectroscopy have been used to characterize the spin states of $Fe^{II}(4,4'\text{-dpb})_2X_2$ (dpb = diphenyl-2,2'-bipyridyl; X = NCS^-, $NCSe^-$) in the temperature range $6 \le T \le 460$ K. Both complexes show a continuous variation of the field-dependent effective magnetic moment over this range. Below ~325 K, both the infrared and Mossbauer spectroscopic signatures are insufficient to permit characterization of the spin state(s) of the metal atom in these complexes, but at higher temperatures, the FTIR data can be accounted for by the increasing population of a high ($S = 2$) spin state, while the Mossbauer spectra can be accounted for by a rapid (on the Mossbauer time scale) relaxation between two spin states. The existence of an intermediate ($S = 1$) spin state for Fe(II) is a consequence of a major distortion from octahedral symmetry of the metal-based orbitals, permitting a (near) degeneracy of the d_{z^2} and d_{xy} levels around this atom.

Introduction

It is well understood that a triplet state ($S = 1$) cannot be the ground state for an iron(II) ion in an ideal octahedral environment due to the degeneracy of the t_{2g} energy levels. However, if the effective ligand field is less than cubic, the possibility of a triplet ground state becomes theoretically possible.[1] $[Fe^{II}([15]ane\text{-}N_4)(NO_2)](PF_6)$, where [15]ane-$N_4$ = 1,4,8,12-tetraazacyclopentadecane, is the single six-coordinated iron(II) complex that has been reported to have a triplet ground state throughout the temperature region studied (96-352 K).[2] This complex is expected to be severely distorted from octahedral symmetry if the nitro group is bonded to the iron atom through both of the oxygen atoms, as suggested by the infrared data reported by these authors. Other claims of such $S = 1$ six-coordinate iron(II) complexes have been reported in the past, but have been retracted, on the basis of further experiments that indicated ground states other than a triplet state.[3] A few four-coordinate Fe^{2+} porphyrins have been reported to be in a triplet ground state on the basis of several experimental techniques,[4a] and a crystal structure has been reported. However, these complexes have a square-planar geometry, and therefore, their triplet state results from, and is different from, the triplet state that would exist in a six-coordinate complex. An intermediate spin state for a five-coordinate Fe(II) reported by Bacci et al.[4b] shows a smooth variation of the magnetic moment between 86 K ($\mu_{eff} = 0.98\ \mu_B$) and 376 K ($\mu_{eff} = 2.26\ \mu_B$).

The synthesis of new complexes that are related to known iron(II) spin-crossover complexes [complexes known to undergo a thermally driven spin-state transition between the high-spin state (HS, $S = 2$) and the low-spin state (LS, $S = 0$)] has been one objective of the present investigation. Such studies have been motivated by an effort to understand the effects that small changes in the microstructure of a complex have on the details of the spin-crossover transitions. Two new complexes have been synthesized: $Fe(4,4'\text{-dpb})_2(NCS)_2$ and $Fe(4,4'\text{-dpb})_2(NCSe)_2$, where 4,4'-dpb is a 4,4'-diphenyl-2,2'-bipyridine. These complexes are related to the well-studied spin-crossover complex $Fe(bpy)_2(NCS)_2$, where bpy = 2,2'-bipyridine. The magnetic and spectroscopic properties of the diphenyl complexes are quite different from those of $Fe(bpy)_2(NCS)_2$. This paper reports and discusses the magnetic, infrared, and ^{57}Fe Mossbauer data for the newly synthesized

* To whom correspondence should be addressed at Rutgers.

(1) (a) Koenig, E.; Schnakig, R. *Theor. Chim. Acta* **1973**, *30*, 205. (b) Boyd, P. D. W.; Buckingham, D. A.; McMeeking, R. F.; Mitra, S. *Inorg. Chem.* **1979**, *18*, 3585. Griffith, J. S. *The Theory of Transition Metal Ions*; Cambridge University Press: London, 1961; p 373.
(2) Watkins, D. D.; Riley, D. P.; Stone, J. A.; Busch, D. H. *Inorg. Chem.* **1976**, *15*, 387.
(3) Koenig, E.; Kannellakopulos, B. *Chem. Phys. Lett.* **1972**, *12*, 485. Koenig, E.; Ritter, G.; Kannellakopulos, B. *J. Chem. Phys.* **1973**, *58*, 3001. Koenig, E.; Ritter, G.; Goodwin, A. *Inorg. Chem.* **1981**, *20*, 3677. Purcell, K.; Yeh, S. M.; Eck, J. S. *Inorg. Chem.* **1977**, *16*, 1708. Edwards, M. P.; Hoff, C. D.; Cumutte, B.; Eck, J. S.; Purcell, K. F. *Inorg. Chem.* **1984**, *23*, 2613.
(4) (a) Medhi, O. K.; Silver, J. *J. Chem. Soc., Chem. Commun.* **1989**, 1199 and references therein. (b) Bacci, M.; Ghiladi, C. A.; Orlandini, A. *Inorg. Chem.* **1984**, *23*, 2798.

0020-1669/91/1330-2535$02.50/0